Ecography

ECOG-02788
Lenoir, J., Hattab, T. and Pierre, G. 2016. Climatic microrefugia under anthropogenic climate change: implications for species redistribution. – Ecography doi: 10.1111/ecog.02788

Supplementary material

Supplementary material

Supplementary material (Appendix ECOG-02788 at <www.oikosoffice.lu.se/appendix>).

Appendix A1. Simulations based on the virtual species *Polystichum virtualis*.

Appendix A2. Physiographically informed geographically weighted regression (GWR) model to downscale maximum temperature of the warmest month (*BIO5*) from 1 km to 25 m resolution across northern France.

Appendix A3. Small-footprint light detection-and-ranging (LiDAR) technology to capture topographic and habitat features at very fine spatial resolution.

Appendix A4. Quantitative review to assess the magnitude of the buffering effect on maximum air temperature during summer time that is either due to topographic (e.g. ravines) or habitat (e.g. trees) features.

Appendix A5. Tests of the respective impacts of topoclimate, the buffering capacity and the local decoupling between sub-canopy and free-air temperatures on the probability for *Polystichum virtualis* to persist locally under a warming scenario of +2°C.

Appendix A1: Simulations based on the virtual species *Polystichum virtualis*.

To illustrate the impact of the local decoupling effect associated to the buffering capacity of potential microrefugia on species distributions, we generated a virtual species (cf. *Polystichum virtualis*) so that its current warm range margin is located in the forest of Compiègne in northern France (Figs. S1-1 & S1-2). Using maximum temperature of the warmest month (*BIO5*) as the single abiotic determinant of the distribution of *P. virtualis* (cf. its fundamental niche) (Fig. S1-1), a symmetric beta response curve (Oksanen and Minchin 2002) was generated using the "virtualspecies" package (Leroy et al. 2015) in R (R Core Team 2015) according to the following equation:

$$p = k(BIO5 - BIO5_{min})^{\alpha}(BIO5_{max} - BIO5)^{\gamma} \quad \text{(eqn 1)}$$

Where p is the probability of presence in a focal pixel unit given the value of the environmental variable *BIO5*. The other five parameters ($BIO5_{min}$, $BIO5_{max}$, k, α and γ) allow modifying the shape of the response curve, where $BIO5_{min}$ and $BIO5_{max}$ are the range margins, k is the scaling parameter adjusting the maximum probability of occurrence and α and γ are used to set the location of the optimum and to modify the skewness and kurtosis of the response curve. For *P. virtualis*, we set these five parameters as follows: $BIO5_{min}$ = 2°C; $BIO5_{max}$ = 25.5°C; $\alpha = \gamma = 0.9$; and $k = 0.0118$ (Fig. S1-1). Here, we assume that *P. virtualis* is a sub-mountainous forest plant species and thus we projected its probability of occurrence given equation 1 (cf. its fundamental niche) within forested habitats solely (cf. its realized niche) (Fig. S1-2). Forested habitats were obtained at a global extent from a 1-km resolution forest cover map produced by the United Nations Food and Agricultural Organization's (FAO 2006), while the Corine Land Cover 2000 database at 25-m resolution across northern France (see Appendix S2) and the canopy cover map derived from LiDAR data at 50-cm resolution across the forest of Compiègne (see Appendix S3) were used at the regional and landscape

scale, respectively. More precisely, we first used equation 1 to map current and future – under a hypothetical scenario +2°C warming (Fig. S1-1) – *P. virtualis* probability of occurrence at the global, regional and landscape scales using the 1-km, 25-m and 50-cm resolution grids of *BIO5* (see Appendices S2 and S3), respectively, thus obtaining the potential distribution. We then overlaid all current and future – assuming no change in forest cover – maps of *P. virtualis* probability of occurrence with global, regional and landscape maps of the distribution of forest habitats (cf. mask layers) to obtain the realized distribution.

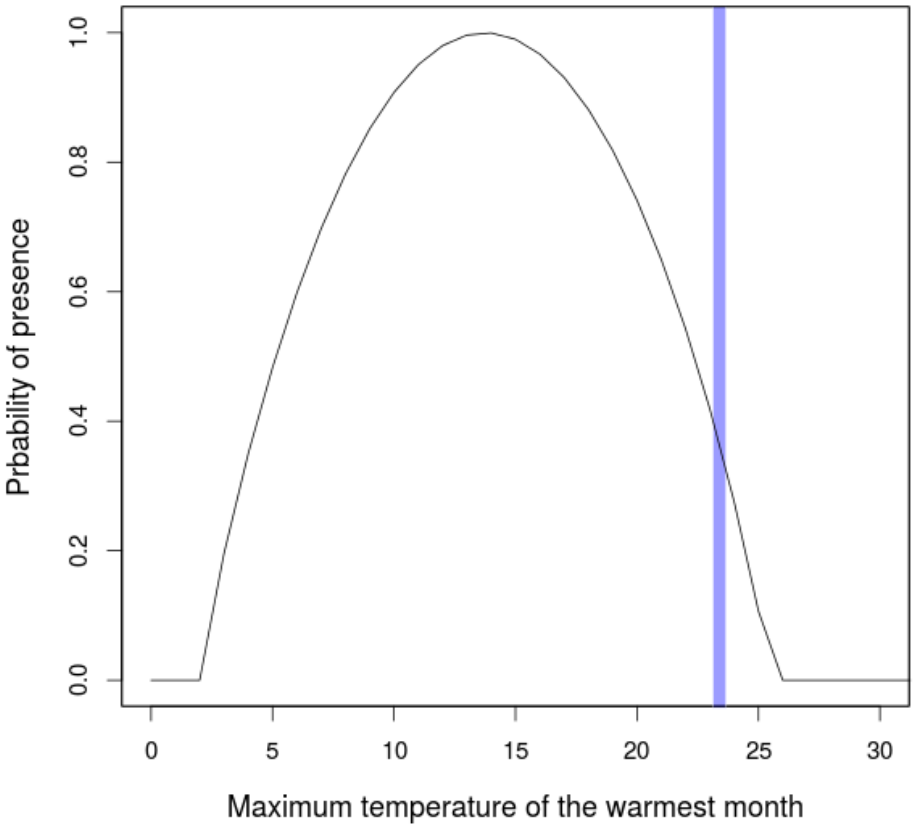

Figure A1-1: Simulated (cf. equation 1) response curve of *Polystichum virtualis* along maximum temperature of the warmest month (*BIO5*). The blue band represent the range of macroclimatic (cf. free-air temperature grid at 1-km resolution) conditions available across the forest of Compiègne under baseline conditions.

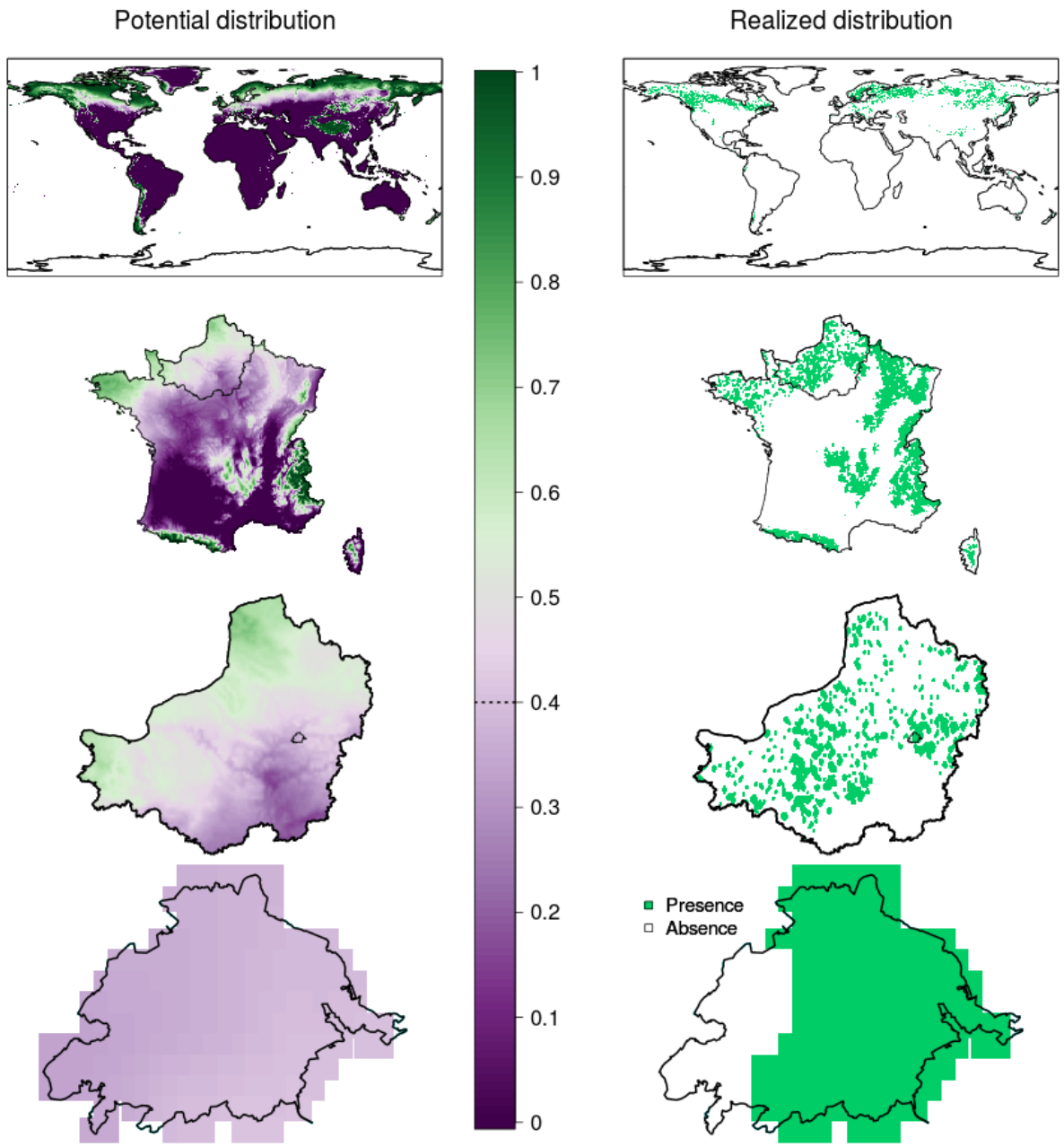

Figure A1-2: Potential and realized distribution of *Polystichum virtualis* at global (1-km resolution across all continents excluding Antarctica) regional (1-km resolution across northern France) and landscape (1-km resolution across the forest of Compiègne) scales. A threshold probability value of 0.4 was used to transform the simulated probabilities of occurrence into presence and absence values.

References

FAO 2006. Global Forest Resources Assessment 2005: Progress towards sustainable forest management. - Food and Agricultural Organization of the United Nations.

Leroy, B. et al. 2015. virtualspecies, an R package to generate virtual species distributions. - Ecography 39: 599–607.

Oksanen, J. and Minchin, P. R. 2002. Continuum theory revisited: what shape are species responses along ecological gradients? - Ecol. Model. 157: 119–129.

R Core Team 2015. R: A Language and Environment for Statistical Computing.

Appendix A2: Physiographically informed geographically weighted regression (GWR) model to downscale maximum temperature of the warmest month (*BIO5*) from 1-km to 25-m resolution across northern France.

Several physiographic variables (Su et al. 2012) known to explain the spatial variability of topoclimate were used as explanatory variables in our GWR model (Ninyerola et al. 2000, Huang et al. 2009, Sears et al. 2011, Luyssaert et al. 2014): (1) altitude; (2) slope; (3) eastness; (4) northness; (5) distance to the sea; (6) monthly average daily clear-sky insolation time; and (7) land cover (see Fig. S2-1). All these variables were derived from a 25-m DEM downloaded from the IGN BD ALTI database (http://professionnels.ign.fr/bdalti) and from the Corine Land Cover 2000 database (http://www.eea.europa.eu: Büttner et al. 2004) using GRASS GIS 7 (Neteler et al. 2012). To compute monthly average daily clear-sky insolation time, we used the algorithm described in Šúri and Hofierka (2004), as implemented in the "r.sun" command running under GRASS GIS 7. It computes clear-sky insolation time (hours) at a daily time step using the model of the European Solar Radiation Atlas (http://www.soda-is.com/esra: Rigollier et al. 2000), which is based on the Linke turbidity coefficient. This command also includes routines to account for hillshading effects caused by variations in solar angle, ground slope, and aspect, as well as shadowing effects of adjacent topographic features. Note that the Linke turbidity coefficient represents the transparency of the cloudless atmosphere by accounting for aerosols and water vapour in the atmosphere. Land cover is the only vector data (polygons) which we rasterized at 25-m resolution across northern France before including it as a factor variable in the model with five levels: (1) artificial surfaces; (2) agricultural areas; (3) forest and semi-natural areas; and (4) wetlands and (5) water bodies.

Based on this large set of physiographic explanatory variables, we ran a GWR model in R (R Core Team 2015) using the "spgwr" package (Bivand and Yu 2015) and setting the optimal bandwidth at 6.8 km to statistically downscale *BIO5* at 25-m resolution across

northern France (Fig. S2-2) and more specifically across the forest of Compiègne (Fig. S2-3). Instead of estimating a set of global regression coefficients using the total numbers of observations across the entire study area, only nearest neighbours of each pixel unit of the temperature grid – *BIO5* here – are used to estimate a set of local regression coefficients. We used a Gaussian weighting function with a fixed bandwidth. The optimal size of the bandwidth of the spatial kernel function was determined by a cross-validation technique which seeks to find a bandwidth minimizing the root mean squared prediction error (RMSPE) of the GWR model (Fotheringham et al. 2002). These model specifications performed very well in respect of the given quasi-global adjusted R^2 of 0.99 and the spatial distribution of local adjusted R^2 values exceeding 0.95 across most of northern France (see Fig. S2-2c) and reaching 0.85 ($\pm 0.24\ 10^{-4}$: standard error of the mean) across the forest of Compiègne.

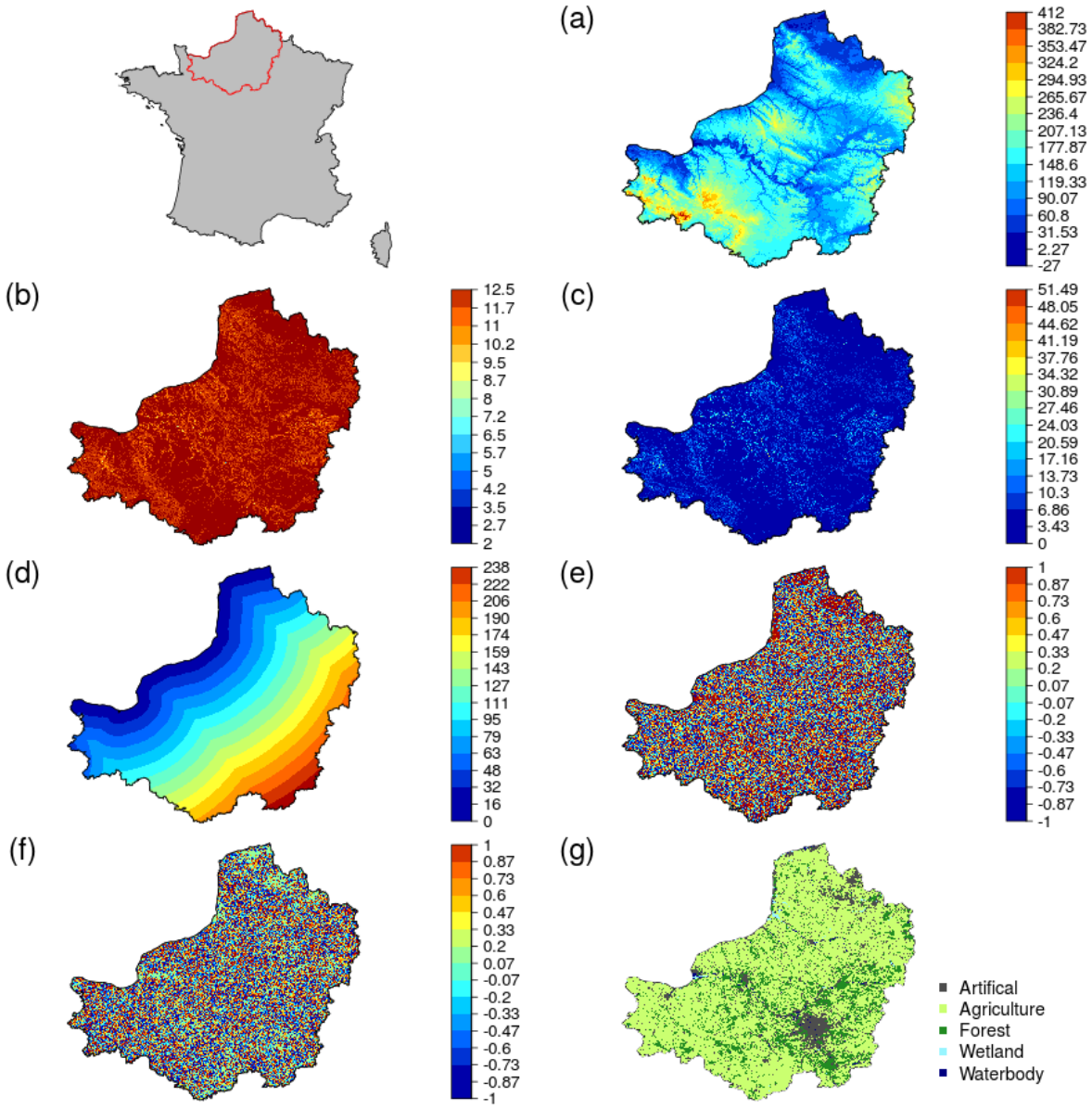

Figure A2-1: Predictor variables used to statistically downscale maximum temperature of the warmest month (*BIO5*) at 25-m resolution across northern France: (a) altitude (m); (b) average insolation time (h); (c) slope (degree); (d) distance to the sea (km); (e) northness index (0-1); (f) eastness index (0-1); and (g) land cover.

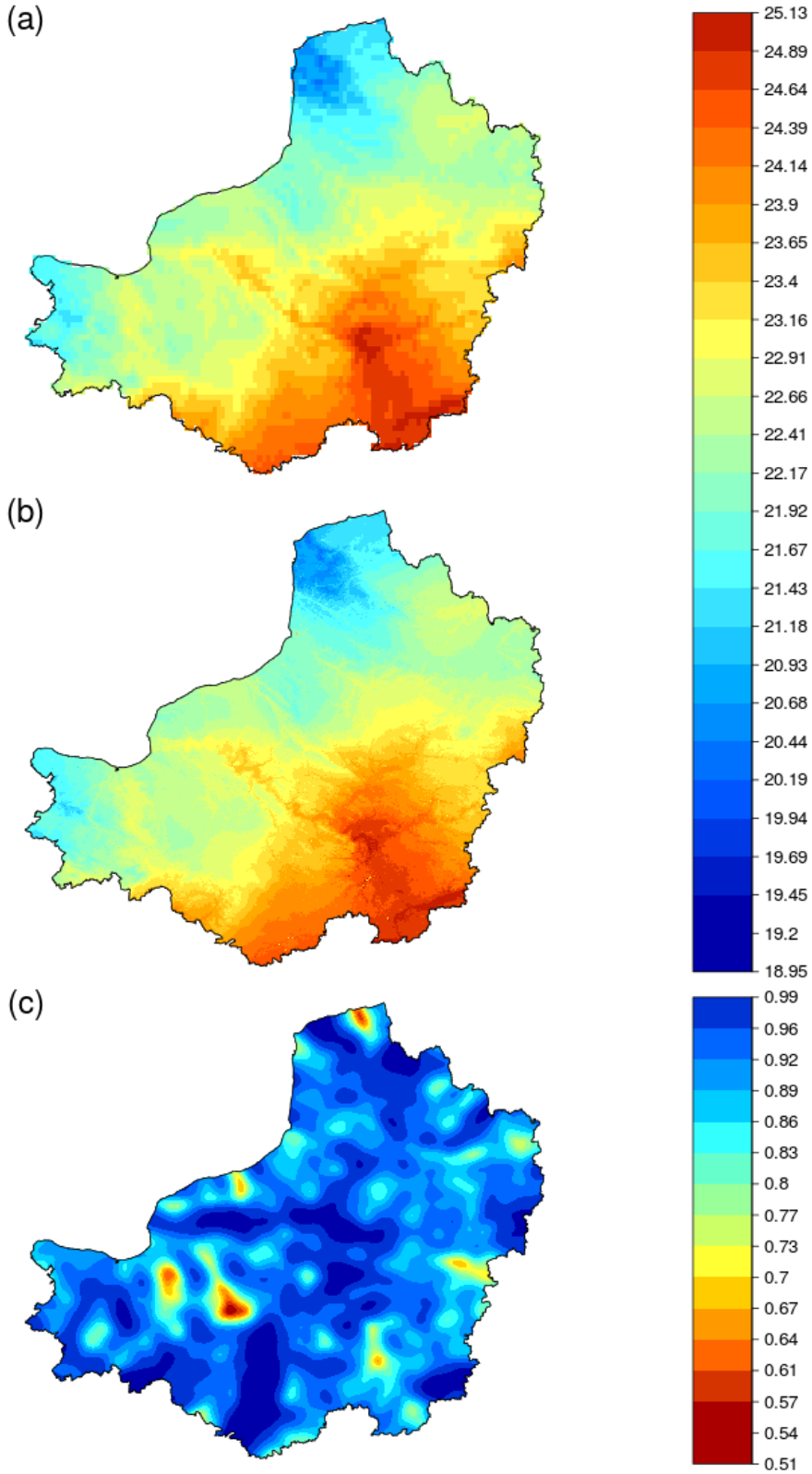

Figure A2-2: Maximum temperature of the warmest month (*BIO5*) at (a) 1-km resolution and (b) 25-m resolution across northern France as well as (c) the spatial distribution of local adjusted R^2 values obtained from a geographically weighted regression (GWR) model.

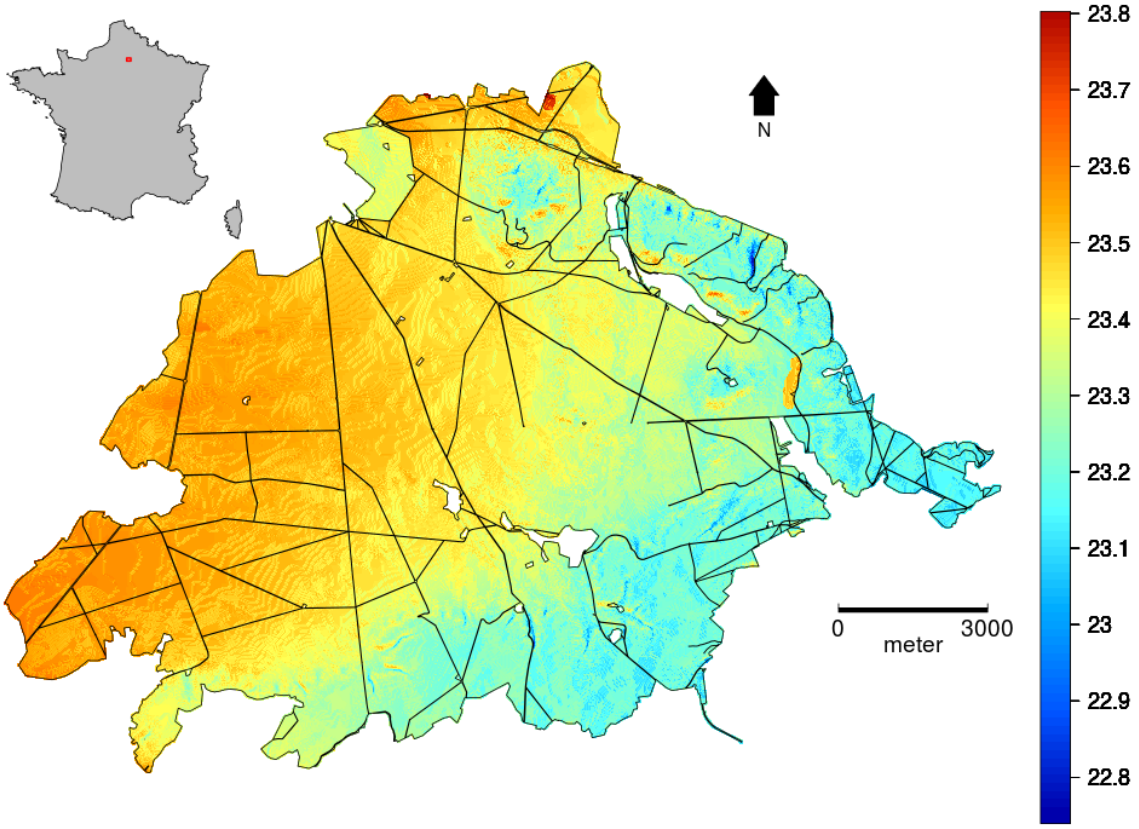

Figure A2-3: Maximum temperature of the warmest month (BIO5) at 25-m resolution across the forest of Compiègne (northern France). This map was generated from a geographically weighted regression (GWR) model.

References

Bivand, R. and Yu, D. 2015. spgwr: Geographically Weighted Regression.

Büttner, G. et al. 2004. The CORINE Land Cover 2000 Project. - EARSeL EProceedings 3: 331–346.

Fotheringham, A. S. et al. 2002. Geographically Weighted Regression: The Analysis of Spatially Varying Relationships. - Wiley-Blackwell.

Huang, S. et al. 2009. Modeling Near-Surface Air Temperature From Solar Radiation and Lapse Rate: New Development on Short-Term Monthly and Daily Approach. - Phys. Geogr. 30: 517–527.

Luyssaert, S. et al. 2014. Land management and land-cover change have impacts of similar magnitude on surface temperature. - Nat. Clim. Change 4: 389–393.

Neteler, M. et al. 2012. GRASS GIS: A multi-purpose open source GIS. - Environ. Model. Softw. 31: 124–130.

Ninyerola, M. et al. 2000. A methodological approach of climatological modelling of air temperature and precipitation through GIS techniques. - Int. J. Climatol. 20: 1823–1841.

R Core Team 2015. R: A Language and Environment for Statistical Computing.

Rigollier, C. et al. 2000. On the clear sky model of the ESRA — European Solar Radiation Atlas — with respect to the heliosat method. - Sol. Energy 68: 33–48.

Sears, M. W. et al. 2011. The World Is not Flat: Defining Relevant Thermal Landscapes in the Context of Climate Change. - Integr. Comp. Biol.: icr111.

Su, Y.-F. et al. 2012. Spatial non-stationarity in the relationships between land cover and surface temperature in an urban heat island and its impacts on thermally sensitive populations. - Landsc. Urban Plan. 107: 172–180.

Šúri, M. and Hofierka, J. 2004. A New GIS-based Solar Radiation Model and Its Application to Photovoltaic Assessments. - Trans. GIS 8: 175–190.

Appendix A3: Small-footprint light detection-and-ranging (LiDAR) technology to capture topographic and habitat features at very fine spatial resolution.

In 2014, the Office National des Forêts (ONF) acquired airborne LiDAR data across the entire lowland forest of Compiègne (144 km^2). The AERODATA Company (http://www.aerodata-france.com/) installed a Riegl LMS-680i laser scanner (http://www.riegl.com/) on a plane and performed flights in February 2014 to get an average density of 12 $points.m^{-2}$. The AERODATA Company also performed the post-processing of the data to calibrate and merge laser bands, to create a raw point cloud and to classify each point as "ground", "vegetation", "water" or "building". Data classification was performed using an automatic ground search algorithm. This routine starts a search procedure to find the lowest last-return points within grid cells of 100 m^2 each (cf. ground points), which are then connected by a triangulated irregular network (TIN). This initial gross TIN is iteratively refined by adding likely ground points that fulfil threshold conditions in terms of distance and angle towards the TIN model. The iterative point addition process is stopped once no more points fulfil the threshold conditions. We then interpolated the points classified as ground returns to create a 50-cm digital terrain model (DTM) comprising 45360 × 45360 cells: about 2 giga-cells. Such very high-resolution (VHR) DTM can provide surrogates for important microclimatic variables such as cold-air drainage or temperature inversions (Leempoel et al. 2015).

To account for cold-air drainage effects, we applied the geomorphons (geomorphologic phonotypes) method based on the principle of pattern recognition to classify and map landforms (Jasiewicz and Stepinski 2013). This method distinguishes 10 different geomorphons: flat; peak; ridge; shoulder; spur; slope; hollow; footslope; valley; and pit. Our VHR DTM was used as input data in the "r.geomorphon" and "r.skyview" commands running under GRASS GIS 7 to (i) identify both the "valley" and "pit" geomorphons (cf. ravines and gullies) whose depth is greater than 5 m and (ii) calculate the sky view factor (SVF),

respectively. SVF values are dimensionless and range from 0 to 1, representing totally obstructed and open spaces, respectively (Watson and Johnson 1987). Previous works have widely used SVF in order to study the relationship between urban elements and microclimatic conditions (e.g. Chen et al. 2012, Scarano and Sobrino 2015). By combining SVF values together with depth values from the "valley" and "pit" geomorphons that are at least 5-m deep, we generated a map of relative topographic concavity that we scaled to range between 0 and 1 (Fig. S3-1).

We also generated a map of canopy density by subtracting elevation values of the LiDAR point-returns classified as "vegetation" from our VHR DTM. Then, we divided the total number of points classified as "vegetation" and which height exceeds 8 m (cf. the canopy layer) by the total number of points classified as "vegetation" within a 50-cm spatial unit, providing us an index of canopy density ranging between 0 and 1 (Fig. S3-1).

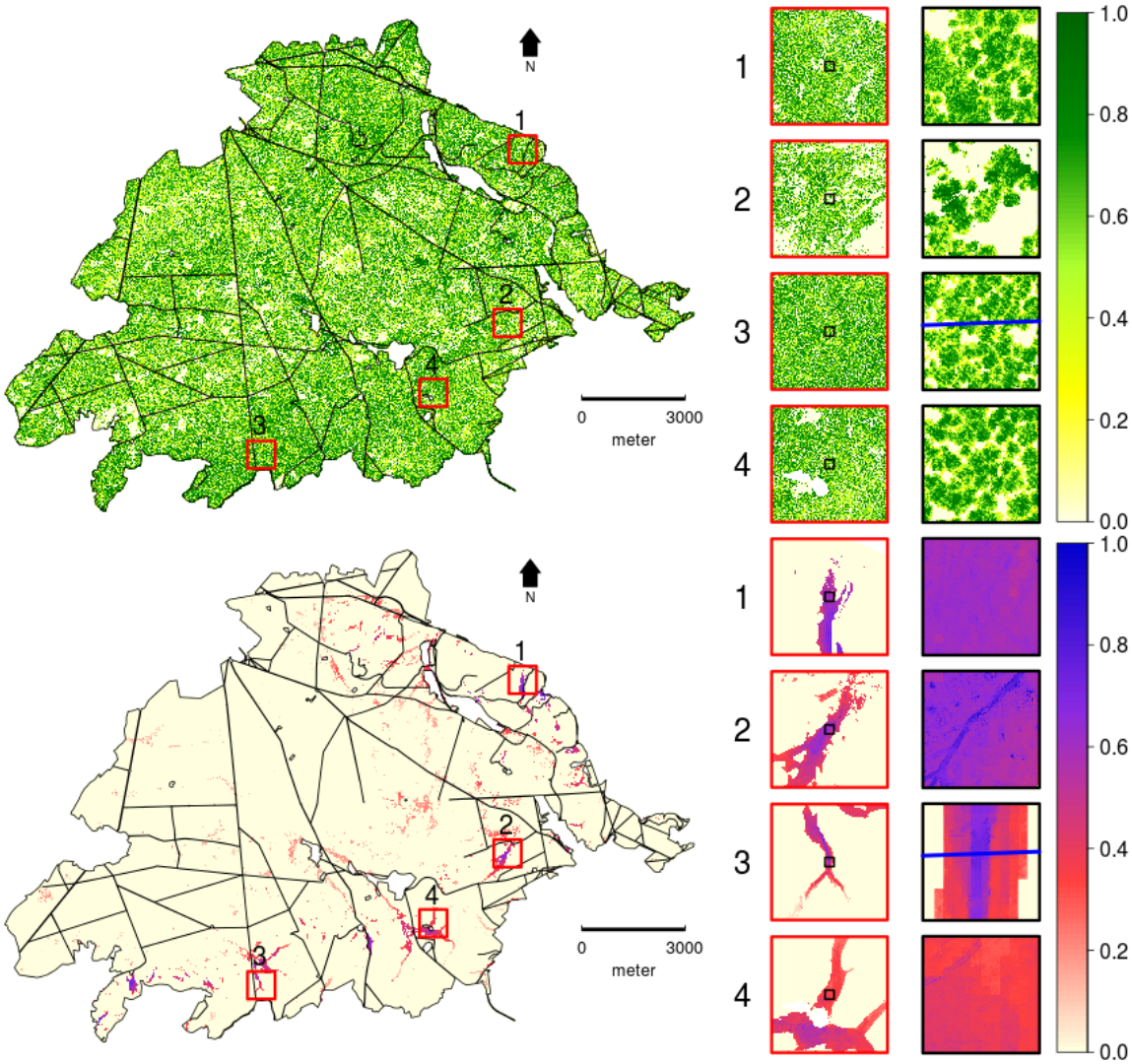

Figure A3-1: Canopy density (cf. the top map and the associated four sets of two cascading zooming windows) and topographic concavity (cf. the bottom map and the associated four sets of two cascading zooming windows) derived at 50-cm resolution across the forest of Compiègne (144 km^2 in northern France) from small-footprint light detection-and-ranging (LiDAR) data. The blue line in zooming window #3 corresponds to the vertical section shown in Figure 6 of the main manuscript.

References

Chen, L. et al. 2012. Sky view factor analysis of street canyons and its implications for daytime intra-urban air temperature differentials in high-rise, high-density urban areas of Hong Kong: a GIS-based simulation approach. - Int. J. Climatol. 32: 121–136.

Jasiewicz, J. and Stepinski, T. F. 2013. Geomorphons — a pattern recognition approach to classification and mapping of landforms. - Geomorphology 182: 147–156.

Leempoel, K. et al. 2015. Very high-resolution digital elevation models: are multi-scale derived variables ecologically relevant? - Methods Ecol. Evol. 6: 1373–1383.

Scarano, M. and Sobrino, J. A. 2015. On the relationship between the sky view factor and the land surface temperature derived by Landsat-8 images in Bari, Italy. - Int. J. Remote Sens. 36: 4820–4835.

Watson, I. D. and Johnson, G. T. 1987. Graphical estimation of sky view-factors in urban environments. - J. Climatol. 7: 193–197.

Appendix A4: Quantitative review to assess the magnitude of the buffering effect on maximum air temperature during summer time that is either due to topographic (e.g. ravines) or habitat (e.g. trees) features.

Focusing on the physiographic and biophysical processes operating at very fine (< 50-m) resolutions, we collated, until June 2016, data from peer-reviewed literature on the magnitude of the buffering effect due to either topographic (e.g. ravines) or habitat (e.g. trees) features. Following the approach used by Scheffers et al. (2014) who reviewed microhabitat-buffering effects for the tropics, we searched in ISI Web of Science and Google Scholar, for the following terms: "microrefugi*" or "microclimat*" or "microhabitat*" or "microenvironment*" and "buffer*" and "temperature*" and "climate" and "topo*" or "canopy". We selected only studies that directly measured microhabitat temperatures from at least two contrasting habitats (e.g. ravine vs. flat or forest vs. open) (e.g. Davies-Colley et al. 2000, Grimmond et al. 2000, Locosselli et al. 2016) or that contrasted microhabitat temperatures with synoptic temperatures (e.g. Renaud and Rebetez 2009, Joly 2014). We paid particular attention to only select papers that had a strict paired design contrasting microhabitat with macrohabitat temperatures (Scheffers et al. 2014). We further constrained our selection to the set of studies focusing on maximum air temperature during the hottest period of the year (i.e. summer months at mid to high latitudes and the dry season in the tropics) to reflect our macroclimatic variable of interest: maximum temperature of the warmest month (*BIO5*) (see Appendix S2). By computing the difference in maximum air temperature during the hottest period of the year between microhabitat and macrohabitat conditions, we were able to assess the magnitude of the buffering effect. If graphs were provided instead of summary statistics (usually reported in Tables or directly in the text of the result section), we used the graph digitizing software WebPlotDigitizer (http://arohatgi.info/WebPlotDigitizer/) to extract temperature data from the graphs. Due to

high variability in figure types and formats, adopting a standardized means for extracting data was not possible (Scheffers et al. 2014). As suggested by Scheffers et al. (2014), we ensured that our data extractions were comparable between microhabitats and paired macrohabitat samples within each study. If raw data were available from a data repository (e.g. Varner and Dearing 2014), we downloaded the data and computed the difference in maximum air temperature during the hottest period of the year between microhabitat and macrohabitat conditions directly in R (R Core Team 2015). In total, we were able to extract data from 21 publications written between 1974 and 2016 from 13 countries (Table S4-1) covering the three main biomes: boreal (n = 1); temperate (n = 11); and tropical (n = 9). Based on this set of data, we found that maximum air temperature during summer time can be reduced, on average (± the standard error of the mean), by 3.2°C (±0.25; n = 23) in temperate deciduous forests. Although not significantly different, we found the buffering effect due to canopy density (-3.5°C ±0.24; n = 18) to be about 1°C greater than the buffering effect due to topographic concavity (-2.3°C ±0.67; n = 5) in temperate deciduous forests.

Reference	ΔT (°C)	H (cm)	Buffer	Forest	CC	Biome
Anderson et al. (2007)	-1.31	100	Stream	Everg.	US	Temp.
Anderson et al. (2007)	-4.50	100	Stream	Everg.	US	Temp.
Anderson et al. (2007)	-10.94	100	Stream	Everg.	US	Temp.
Anderson et al. (2007)	-4.62	100	Stream	Everg.	US	Temp.
Anderson et al. (2007)	-5.76	100	Stream	Everg.	US	Temp.
Anderson et al. (2007)	-1.57	100	Stream	Everg.	US	Temp.
Carlson and Groot (1997)	-3.80	15	Canopy	Decid.	CA	Bor.
Chen et al. (1999)	-1.90	200	Canopy	Everg.	US	Temp.
Davies-Colley et al. (2000)	-1.50	150	Canopy	Everg.	NZ	Trop.
de Freitas and Enright (1995)	-3.50	150	Canopy	Everg.	NZ	Trop.
de Freitas and Enright (1995)	-1.40	150	Canopy	Everg.	NZ	Trop.
Delgado et al. (2007)	-2.84	0	Canopy	Everg.	ES	Trop.
Delgado et al. (2007)	-1.13	0	Canopy	Everg.	ES	Trop.
Delgado et al. (2007)	-4.19	0	Canopy	Everg.	ES	Trop.
Delgado et al. (2007)	-1.31	0	Canopy	Everg.	ES	Trop.
Delgado et al. (2007)	-3.81	5	Canopy	Everg.	ES	Trop.
Delgado et al. (2007)	-3.91	5	Canopy	Everg.	ES	Trop.
Delgado et al. (2007)	-2.44	5	Canopy	Everg.	ES	Trop.
Delgado et al. (2007)	+0.48	5	Canopy	Everg.	ES	Trop.
Delgado et al. (2007)	-2.85	130	Canopy	Everg.	ES	Trop.
Delgado et al. (2007)	-2.80	130	Canopy	Everg.	ES	Trop.
Delgado et al. (2007)	-1.30	130	Canopy	Everg.	ES	Trop.
Delgado et al. (2007)	+0.44	130	Canopy	Everg.	ES	Trop.
Denslow (1980)	-5.20	100	Canopy	Everg.	EC	Trop.
Ewers and Banks-Leite (2013)	-9.94	100	Canopy	Everg.	BR	Trop.
Godefroid et al. (2006)	-2.50	100	Canopy	Decid.	BE	Temp.
Grimmond et al. (2000)	-2.20	250	Topo	Decid.	US	Temp.
Grimmond et al. (2000)	-1.80	250	Topo	Decid.	US	Temp.
Johansson (1974)	-5.00	100	Canopy	Everg.	LR	Trop.
Joly (2014)	-3.10	150	Canopy	Everg.	FR	Temp.
Joly (2014)	-2.10	150	Canopy	Mixed	FR	Temp.
Joly (2014)	-3.60	150	Canopy	Decid.	FR	Temp.
Korb and Linsenmair (1998)	-3.10	50	Canopy	Everg.	CI	Trop.
Locosselli et al. (2016)	-0.70	150	Canopy	Everg.	BR	Trop.
Locosselli et al. (2016)	-4.20	150	Topo	Everg.	BR	Trop.
Locosselli et al. (2016)	-2.40	150	Topo	Everg.	BR	Trop.
Locosselli et al. (2016)	-1.80	150	Topo	Everg.	BR	Trop.
Morecroft et al. (1998)	-3.00	200	Canopy	Decid.	UK	Temp.
Potter et al. (2001)	-5.70	50	Canopy	Decid.	US	Temp.
Potter et al. (2001)	-4.70	50	Canopy	Decid.	US	Temp.
Potter et al. (2001)	-3.20	50	Canopy	Decid.	US	Temp.
Potter et al. (2001)	-2.70	50	Canopy	Decid.	US	Temp.
Renaud and Rebetez (2009)	-4.80	200	Canopy	Decid.	CH	Temp.
Renaud and Rebetez (2009)	-4.72	200	Canopy	Mixed	CH	Temp.
Renaud and Rebetez (2009)	-4.00	200	Canopy	Mixed	CH	Temp.
Renaud and Rebetez (2009)	-3.81	200	Canopy	Decid.	CH	Temp.
Renaud and Rebetez (2009)	-3.53	200	Canopy	Mixed	CH	Temp.
Renaud and Rebetez (2009)	-3.16	200	Canopy	Decid.	CH	Temp.
Renaud and Rebetez (2009)	-2.99	200	Canopy	Mixed.	CH	Temp.

Renaud and Rebetez (2009)	-2.70	200	Canopy	Decid.	CH	Temp.
Renaud and Rebetez (2009)	-2.47	200	Canopy	Everg.	CH	Temp.
Renaud and Rebetez (2009)	-2.26	200	Canopy	Everg.	CH	Temp.
Renaud and Rebetez (2009)	-2.01	200	Canopy	Decid.	CH	Temp.
Renaud and Rebetez (2009)	-1.29	200	Canopy	Everg.	CH	Temp.
Renaud and Rebetez (2009)	+0.46	200	Canopy	Everg.	CH	Temp.
Renaud and Rebetez (2009)	+0.54	200	Canopy	Everg.	CH	Temp.
Shoo et al. (2010)	-8.84	70	Canopy	Mixed	AU	Trop.
Varner and Dearing (2014)	-6.77	200	Canopy	Everg.	US	Temp.
Varner and Dearing (2014)	-5.15	200	Canopy	Everg.	US	Temp.
von Arx et al. (2012)	-0.43	200	Canopy	Everg.	CH	Temp.
von Arx et al. (2012)	0.29	200	Canopy	Everg.	CH	Temp.
von Arx et al. (2012)	-0.65	200	Canopy	Everg.	CH	Temp.
von Arx et al. (2012)	-0.73	200	Canopy	Everg.	CH	Temp.
von Arx et al. (2012)	-0.50	200	Canopy	Everg.	CH	Temp.
von Arx et al. (2012)	-2.73	200	Canopy	Everg.	CH	Temp.
von Arx et al. (2012)	-3.35	200	Canopy	Everg.	CH	Temp.
von Arx et al. (2012)	-2.84	200	Canopy	Everg.	CH	Temp.
von Arx et al. (2012)	-1.56	200	Canopy	Everg.	CH	Temp.
von Arx et al. (2012)	-2.18	200	Canopy	Everg.	CH	Temp.
von Arx et al. (2012)	-1.53	200	Canopy	Everg.	CH	Temp.
von Arx et al. (2012)	-3.22	200	Canopy	Decid.	CH	Temp.
von Arx et al. (2012)	-3.34	200	Canopy	Decid.	CH	Temp.
von Arx et al. (2012)	-3.57	200	Canopy	Decid.	CH	Temp.
von Arx et al. (2012)	-2.46	200	Canopy	Decid.	CH	Temp.
von Arx et al. (2012)	-2.95	200	Canopy	Decid.	CH	Temp.
von Arx et al. (2012)	-5.09	200	Canopy	Decid.	CH	Temp.
Xu et al. (1997)	-3.86	100	Topo	Decid.	US	Temp.
Xu et al. (1997)	-0.19	100	Topo	Decid.	US	Temp.
Xu et al. (1997)	-3.67	100	Topo	Decid.	US	Temp.

Table A4-1: A list of 21 studies (by alphabetic order) selected by our literature search and reporting buffering effects due to either topographic features, canopy cover or distance to a stream. See corresponding reference list below. ΔT (°C) is the difference in maximum air temperature during the hottest period of the year between microhabitat and macrohabitat conditions. H (cm) is the height at which microsensors have been mounted to measure air temperature. Buffer indicates the type of buffering effect (topography, canopy or stream). Forest is the type of forest habitat (deciduous, evergreen or mixed). CC is the country code. The three main biomes (boreal, temperate and tropical) are represented.

References

Anderson, P. D. et al. 2007. Riparian buffer and density management influences on microclimate of young headwater forests of Western Oregon. - For. Sci. 53: 254–269.

Carlson, D. W. and Groot, A. 1997. Microclimate of clear-cut, forest interior, and small openings in trembling aspen forest. - Agric. For. Meteorol. 87: 313–329.

Chen, J. et al. 1999. Microclimate in Forest Ecosystem and Landscape Ecology Variations in local climate can be used to monitor and compare the effects of different management regimes. - BioScience 49: 288–297.

Davies-Colley, R. J. et al. 2000. Microclimate gradients across a forest edge. - N. Z. J. Ecol. 24: 111–121.

de Freitas, C. R. and Enright, N. J. 1995. Microclimatic differences between and within canopy gaps in a temperate rainforest. - Int. J. Biometeorol. 38: 188–193.

Delgado, J. D. et al. 2007. Edge effects of roads on temperature, light, canopy cover, and canopy height in laurel and pine forests (Tenerife, Canary Islands). - Landsc. Urban Plan. 81: 328–340.

Denslow, J. S. 1980. Gap Partitioning among Tropical Rainforest Trees. - Biotropica 12: 47–55.

Ewers, R. M. and Banks-Leite, C. 2013. Fragmentation Impairs the Microclimate Buffering Effect of Tropical Forests. - PLOS ONE 8: e58093.

Godefroid, S. et al. 2006. Spatial variability of summer microclimates and plant species response along transects within clearcuts in a beech forest. - Plant Ecol. 185: 107–121.

Grimmond, C. S. B. et al. 2000. Spatial variability of micro-climatic conditions within a mid-latitude deciduous forest. - Clim. Res. 15: 137–149.

Johansson, D. 1974. Ecology of vascular epiphytes in West African rain forest. 59: 1–124.

Joly, D. 2014. Etude comparative de la température en forêt et en espace ouvert dans le parc naturel régional du Haut-Jura. - Climatologie 11: 19–33.

Korb, J. and Linsenmair, K. E. 1998. The effects of temperature on the architecture and distribution of Macrotermes bellicosus (Isoptera, Macrotermitinae) mounds in different habitats of a West African Guinea savanna. - Insectes Sociaux 45: 51–65.

Locosselli, G. M. et al. 2016. Rock outcrops reduce temperature-induced stress for tropical conifer by decoupling regional climate in the semiarid environment. - Int. J. Biometeorol. 60: 639–649.

Morecroft, M. D. et al. 1998. Air and soil microclimates of deciduous woodland compared to an open site. - Agric. For. Meteorol. 90: 141–156.

Potter, B. E. et al. 2001. The impact of forest structure on near-ground temperatures during two years of contrasting temperature extremes. - Agric. For. Meteorol. 106: 331–336.

R Core Team 2015. R: A Language and Environment for Statistical Computing.

Renaud, V. and Rebetez, M. 2009. Comparison between open-site and below-canopy climatic conditions in Switzerland during the exceptionally hot summer of 2003. - Agric. For. Meteorol. 149: 873–880.

Scheffers, B. R. et al. 2014. Microhabitats in the tropics buffer temperature in a globally coherent manner. - Biol. Lett. 10: 20140819.

Shoo, L. P. et al. 2010. Potential for mountaintop boulder fields to buffer species against extreme heat stress under climate change. - Int. J. Biometeorol. 54: 475–478.

Varner, J. and Dearing, M. D. 2014. The Importance of Biologically Relevant Microclimates in Habitat Suitability Assessments. - PLOS ONE 9: e104648.

von Arx, G. et al. 2012. Spatio-temporal effects of forest canopy on understory microclimate in a long-term experiment in Switzerland. - Agric. For. Meteorol. 166–167: 144–155.

Xu, M. et al. 1997. Temperature and its variability in oak forests in the southeastern Missouri Ozarks. - Clim. Res. 8: 209–223.

Appendix A5: Tests of the respective impacts of topoclimate, the buffering capacity and the local decoupling between sub-canopy and free-air temperatures on the probability for *Polystichum virtualis* to persist locally under a warming scenario of +2°C.

	Topo	Micro (B)	Micro (B+D)
Macro	0.27	<< 0.001	<< 0.001
Topo	-	<< 0.001	<< 0.001
Micro (B)	-	-	<< 0.001

Table A3-1: Matrix of *p.values* from all possible pairwise comparisons between the four sets (Macro, Topo, Micro (B) and Micro (B+D)) of probability of occurrence values of *Polystichum virtualis* obtained under a warming scenario of +2°C (cf. Table 1). Student *t*-tests were used. See Table 1 for the meaning of Macro, Topo, Micro (B) and Micro (B+D).